Using Dynamic Responses of Moving Vehicles to Extract Bridge Modal Properties of a Field Bridge

Xuan Kong, A.M.ASCE[1]; C. S. Cai, F.ASCE[2]; Lu Deng, M.ASCE[3]; and Wei Zhang, M.ASCE[4]

Abstract: The vehicles moving on a bridge excite bridge vibration and can also serve as response receivers because the vehicle dynamic response contains the vibration information of the bridge. A methodology was proposed in a previous study for extracting bridge modal properties, such as natural frequencies and modal shapes, from the vehicle dynamic responses. A specialized test vehicle consisting of a tractor and two following trailers was developed in which the two trailers towed by the tractor moving along the bridge were used as the dynamic response receivers. The responses of one trailer with a time shift were subtracted from the responses of the other to obtain the residual responses that were then processed with fast Fourier transformation (FFT) and short-time Fourier transformation (STFT) to extract the bridge modal properties. In the present paper, field test data of an existing bridge were adopted to verify the proposed methodology. In the vehicle and bridge system, a bridge finite-element (FE) model was updated using the measured accelerations and strains of the bridge; two types of test vehicle models were proposed for use in simulations of the tractor–trailer test system; and the measured surface-roughness profile was used in the numerical simulation. Parametric studies have been conducted to determine the trailer mass and stiffness. Vehicle Model I shows a good capacity for extracting bridge frequencies and the first two modal shapes with a dominant vertical component. However, Vehicle Model II performed better than Vehicle Model I on the extraction of bridge modal shapes that are dominant in lateral bending. **DOI: 10.1061/(ASCE)BE.1943-5592.0001038.**

Author keywords: Moving vehicle; Vehicle dynamic responses; Field bridge; Bridge modal properties; Tractor and trailer test vehicle; Residual response.

Introduction

Vibration-based damage-detection methods are widely used to identify structural bridge damage by measuring the changes of modal properties such as natural frequencies, modal shapes, and modal damping (Doebling et al. 1998; Sohn et al. 2003; Fan and Qiao 2011; Das et al. 2016). In the existing methods, the measurement data are obtained mostly from sensors directly attached to bridge structures. Although bridge natural frequencies can be obtained easily with one or more sensors, a more complicated experimental plan of a sensor network is required to obtain measurements such as modal shapes and frequency response functions (FRFs) (Carden and Fanning 2004). The entire process involves sensor installation on the bridge, traffic interruption, external excitation, etc., which is typically very time-consuming. However, in an interaction system consisting of a vehicle and a bridge, the instrumented vehicle, which serves as the excitation for system vibration, also can be used as a response receiver. In addition, the measurement of vehicle dynamic responses, such as acceleration, is more convenient in the real world than are modal shapes and FRFs of the bridge.

Because the vehicle dynamic responses contain the vibration information of the bridge, many researchers have proposed using such information for damage detection, model updating, health monitoring, and condition assessment of bridge structures (Bu et al. 2006; Lu et al. 2009, 2010; Lu and Liu 2011; Kong et al. 2014; Malekjafarian et al. 2015). However, most research has been limited to theoretical or numerical investigations and is not ready for application. The most practical research identified bridge frequencies. The feasibility of identifying bridge frequencies from the dynamic responses of an instrumented vehicle moving on a bridge was theoretically studied and validated by Yang et al. (2004) and McGetrick et al. (2009). A parametric study on the effect of key factors was also conducted (Yang and Chang 2009a), and this method was tested using a two-wheel cart towed by a light truck passing over a field bridge (Lin and Yang 2005; Yang and Chang 2009b; Yang et al. 2013). By processing the dynamic responses recorded from an accelerometer installed on the cart, the fundamental frequency of the bridge was obtained. Kim et al. (2011), McGetrick et al. (2013), and Keenahan et al. (2014) set up a laboratory experiment with a scaled bridge and moving vehicles and investigated the feasibility of using an instrumented vehicle to identify the bridge natural frequency, structural damping, dynamic axle force, and road profile. On the basis of an experimental study, González et al. (2008) concluded that the accurate determination of bridge frequency is feasible only when the vehicle velocity is low and the dynamic excitation of the bridge vibration is sufficiently high. It is noteworthy that using frequency shifts to detect damages has practical limitations, especially for large structures (Curadelli et al. 2008). In addition to identification of bridge properties, Keenahan et al. (2014) and González et al. (2012) investigated methods to identify bridge damping using a truck–trailer drive-by system.

[1]Formerly, Research Assistant, Dept. of Civil and Environmental Engineering, Louisiana State Univ., Baton Rouge, LA 70803.

[2]Edwin B. and Norma S. McNeil Distinguished Professor, Dept. of Civil and Environmental Engineering, Louisiana State Univ., Baton Rouge, LA 70803 (corresponding author). E-mail: cscai@lsu.edu

[3]Professor, College of Civil Engineering, Hunan Univ., Changsha, Hunan 410082, China.

[4]Assistant Professor, Dept. of Civil and Environmental Engineering, Univ. of Connecticut, Storrs, CT 06269.

Note. This manuscript was submitted on July 6, 2016; approved on December 5, 2016; published online on March 14, 2017. Discussion period open until August 14, 2017; separate discussions must be submitted for individual papers. This paper is part of the ***Journal of Bridge Engineering***, © ASCE, ISSN 1084-0702.

Miyamoto and Yabe (2011) used the vibration data obtained from a public bus equipped with vibration-measurement instrumentation to assess existing bridge conditions. Zhang et al. (2012, 2013) proposed using the squares of the structural modal shapes extracted from acceleration of a moving tapping vehicle to detect structural damage, and they also developed a method using the curvature of the operating deflection shape.

The vehicle dynamic response contains three groups of frequency components: vehicle frequencies, bridge-related frequencies, and driving-related frequencies (Yang and Chang 2009a). In the Fourier spectra of vehicle dynamic responses, a dominant peak usually appears at the vehicle's fundamental frequency, which makes the identification of bridge frequencies very difficult (Yang et al. 2013). Also, other factors, such as the road-surface roughness and driving-related effects, will affect the identification. Therefore, Yang et al. (2012) proposed using two connected vehicles to reduce such effects and thereby successfully identify the bridge frequencies. Meanwhile, the authors (Kong et al. 2016) proposed a methodology to eliminate the effect of those factors and efficiently extract the bridge frequencies and modal shape squares (MSSs) from the vehicle responses. In their method, a specialized test vehicle consisting of a tractor and two following trailers was developed; the two trailers towed by the tractor moving along the bridge were used as the dynamic response receivers. The residual response of the two trailers was derived theoretically and verified with numerical analyses on a simple structure. In the present paper, the objective is to verify the proposed methodology using field test data from an existing bridge, including accelerations and strains of the bridge and the actual profile of road-surface roughness. In this study, two comprehensive vehicle models are proposed to simulate the test vehicle, and their performances are compared to apply to the design of a vehicle for field applications.

Methodology

During the interaction between vehicles and a bridge, the vehicle dynamic response is dominant with three groups of frequency characteristics: vehicle-related frequencies, bridge-related frequencies, and driving-related frequencies, including the road-surface roughness effect (Yang and Chang 2009a). To extract bridge dynamic properties, the authors developed a methodology using a specialized test vehicle consisting of a tractor and two following trailers (Kong et al. 2016). The tractor was an exciter and hauler was used to actuate bridge vibrations and tow the trailers traveling along the bridge, while the two trailers were instrumented with sensors, which functioned as response receivers similar to moving sensors. To reduce the effect of the trailer self-vibration, the two trailers were designed in a special configuration such that the major components of the trailer responses were caused by bridge vibration. If the two trailers are identical and their distance is constant while moving on the bridge, the responses of the two trailers could be closely correlated. Therefore, the residual responses, namely, the responses of one trailer with a time shift subtracted from the responses of the other, could eliminate the driving-related and road-surface roughness effects. From the residual responses obtained in such way, the modal properties of the bridge can be extracted more reliably and efficiently. A simplified vehicle and bridge coupled (VBC) system was used to simply demonstrate this methodology (Fig. 1). The specialized test vehicle consists of a tractor, V0, and two identical trailers, V1 and V2, towed by the tractor. The distance between the tractor (V0) and the first trailer (V1), $d1$, and the distance between the two trailers, d, are both constants. Sensors such as accelerometers were installed on the two trailers to record the vehicles' vibration responses.

In terms of the VBC analysis, the vertical displacements of the two trailers can be derived as

$$d_{vi}(t) = \sum_{j=1}^{\infty}\left[A_1 \cos\frac{(j-1)\pi x_i}{L} - A_2 \cos\frac{(j+1)\pi x_i}{L} + A_3 \cos\omega_{vi}t - A_4 \cos\left(\omega_j t - \frac{j\pi x_i}{L}\right) + A_5 \cos\left(\omega_j t + \frac{j\pi x_i}{L}\right)\right] + \frac{r'(x_i)}{\omega_{vi}} + r(x_i), \quad i = 1,2 \tag{1}$$

where ω_{vi}^2 and $i = 1,2$ = fundamental frequencies of the two trailers; ω_j = bridge natural frequencies; and $r(x_i)$ and $r'(x_i)$ = road-surface roughness and its derivation at the trailer position, respectively. For information on A_1 to A_5 and other details, see Kong et al. (2016). In Eq. (1), the two rightmost terms are attributed to road roughness, which is independent of other effects on trailer response. Therefore, subtracting the response of one trailer from that of the other could remove the road-roughness effect. The residual displacement of the two trailers can be expressed as

$$\Delta d_{12}(t) = d_{v1}(t) - d_{v2}\left(t + \frac{d}{V}\right) \tag{2}$$

where d_{v1} and d_{v2} = displacements of the two trailers, respectively. Herein, a time shift is introduced in the displacement of the second trailer because a time difference exists when the two trailers pass the same location one after the other. The residual acceleration of the two trailers can be obtained easily by doubly differentiating Eq. (2), which is more applicable because the vehicle acceleration is much easier to measure in the field than the vehicle displacement.

The procedure for extracting bridge modal properties from the trailers' responses is shown in Fig. 2. First, the dynamic responses of

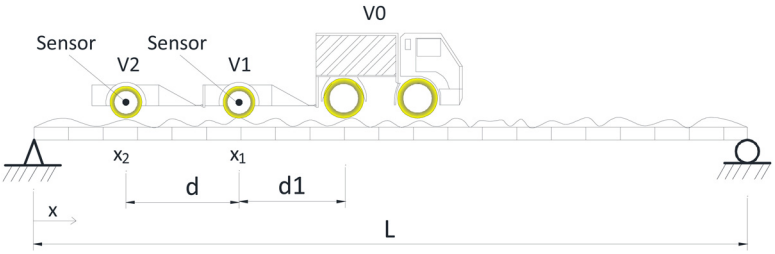

Fig. 1. Configuration of the test vehicle

J. Bridge Eng., 2017, 22(6): -1--1

the two trailers, such as acceleration time histories, $R1(t)$ and $R2(t)$, were measured by the test. The effective data length was determined from the instant the first trailer entered the bridge to the instant the second trailer left the bridge. The time difference of the two trailers was d/v, where v is vehicle speed. Then, to obtain the residual response, the response of the second trailer with the time shift was subtracted from the response of the first trailer, as shown in Fig. 2. Finally, the fast Fourier transformation (FFT) technique was applied to the residual response, and the bridge frequencies were obtained by picking the amplitude peaks after eliminating the vehicle frequencies. In addition, the short-time Fourier transformation (STFT) method was applied to obtain the frequency–time spectra of the residual response and the MSSs of the bridge were extracted. More details of the entire process can be found in Kong et al. (2016).

It is noteworthy that in vehicle and bridge interaction systems, there are many complicating features, such as Coriolis forces, uncertain boundary conditions, three-dimensional (3D) behavior of bridge and vehicle systems, and nonlinearity. However, under real service conditions, the effects of these factors, such as nonlinearity, are not severe, and most researchers study the real world on the basis of assumptions that approximate the real situation. As such, the normal mode assumption is considered reasonable and has been used in numerous applications to reduce the computational effort. Using a case study of field bridges as in the present study is one way to examine all the assumptions.

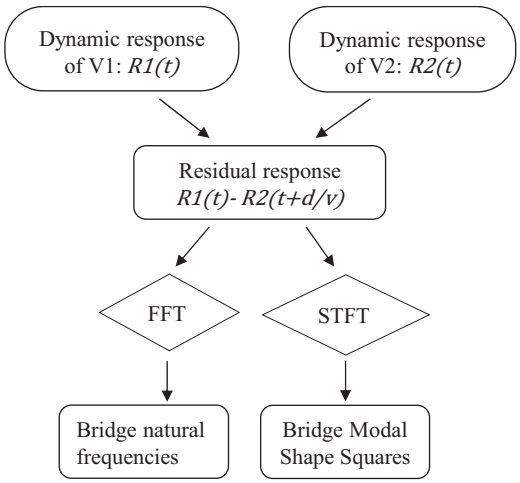

Fig. 2. Procedure for extracting bridge modal properties

Bridge Description and Field Test

For this study, field bridge was introduced to verify the proposed methodology. Both static and dynamic tests were conducted on the bridge in 2006, and strains and accelerations of the bridge were measured (Cai et al. 2007; Deng and Cai 2011). However, measurements of vehicle responses are not available because they were not among the objectives of the test. Meanwhile, a finite-element (FE) model of the bridge was built and updated using field measurement data. Then, the updated bridge FE model, together with the measured road-surface roughness profile, was used to simulate the field bridge.

The test bridge, which crosses over Cypress Bayou in District 61, on LA 408 East, Louisiana, is a two-way bridge with three straight simple spans with a length of 16.764 m (55 ft) each. The bridge consists of two separate structures that carry traffic in opposite directions, and the field test was conducted only on one structure with two lanes. The bridge deck section is not symmetric; it is supported with seven AASHTO Type II prestressed concrete girders spaced 2.13 m (7 ft) from center to center, as shown in Fig. 3. Herein, only the third span of the bridge was instrumented. Seven measurement stations, one for each girder, were installed with strain gauges and accelerometers. On the basis of the bridge configuration, a bridge FE model was created using the *ANSYS 14.5* program and then updated using the first three measured natural frequencies and strains on the seven girders. More details can be found in Deng and Cai (2010). The first three measured bridge frequencies were 8.19 , 11.11, and 15.79 Hz, and the corresponding frequencies of the updated bridge model were 8.19, 10.79, and 16.23 Hz, respectively. The numerical values match the measurement results quite well. Therefore, the updated bridge model was adopted for the present study, and the corresponding frequencies are regarded as true values in the following discussion.

Road-surface roughness of the bridge deck, measured using a laser profiler, included the longitudinal road-surface profile along each wheel track. Herein, a two-dimensional (2D) road-surface profile was used without consideration of changes in road elevation along the lateral direction. To excite the dynamic effect of the vehicle, two wooden bumps, named *Bump 1* and *Bump 2*, with equal widths of 0.18 m and heights of 0.025 m (1 in.) and 0.038 m (1.5 in.) were used. The two wooden bumps, one at a time, were placed at the entrance of the third span. Fig. 4 shows the measured road-surface profile of Lane 1 with the wooden Bump 1 along the track of the right wheel of the test truck. The vehicle used in the bridge field test was a dump truck with a single front axle and a two-axle group in the rear (Deng and Cai 2011). The static weights for the

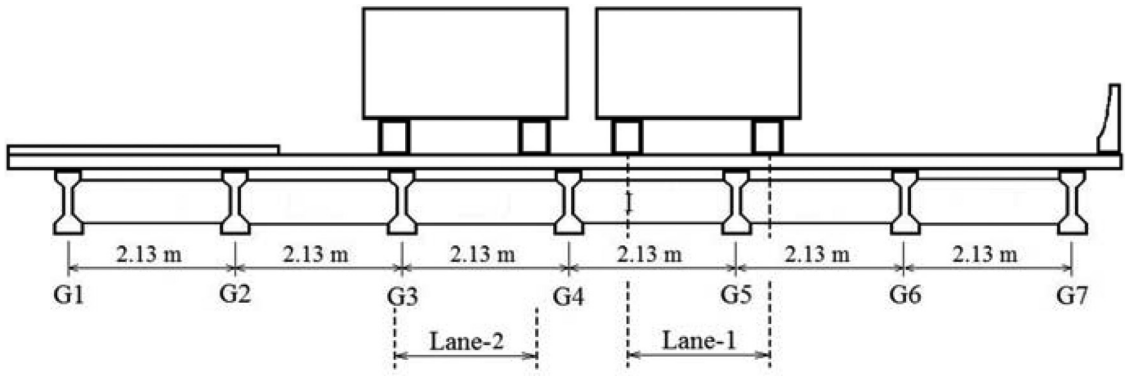

Fig. 3. Bridge cross section and vehicle lane position

J. Bridge Eng., 2017, 22(6): -1--1

first, second, and third axle of this truck were 80.0, 95.6, and 95.6 kN, respectively. The distance between the front axle and the center of the two rear axles was 6.25 m, and the distance between the two rear axles was 1.2 m.

Extraction Using a Simple Test Vehicle (Model I)

Numerical Model of the Test Vehicle

To simulate the proposed tractor–trailer test vehicle as previously described herein and to take advantage of the dump truck used in the field test, a numerical vehicle model is proposed. As shown in Fig. 5, by grouping the rear two axles into an axle group, the three-axle dump truck was modeled as a two-axle vehicle for the tractor, and a single-degree-of-freedom (SDOF) mass-spring-dashpot system was used for each trailer. The main parameters of the truck model are assumed on the basis of the measured data (Table 1). The tractor traveled along Lane 1 and its left wheels were 6.62 m to the right shoulder while the right wheels were 4.42 m to the shoulder (Fig. 3). The first (front) SDOF trailer was connected to the right rear wheel of the tractor and followed by the second (rear) trailer (Fig. 5). The connections between the tractor and the first trailer and between the two trailers were pinned, which means the DOF of the two trailers were independent. The SDOF trailer models were assumed to have the same physical parameters as those of the tractor front wheel, i.e., m_v was 725.4 kg, k_v was 8.0×10^4 N/m, and c_v was 2,189.6 kg/s. The mass of the trailer was very small compared to the mass of dump truck, and the frequency of the trailer was 1.67 Hz.

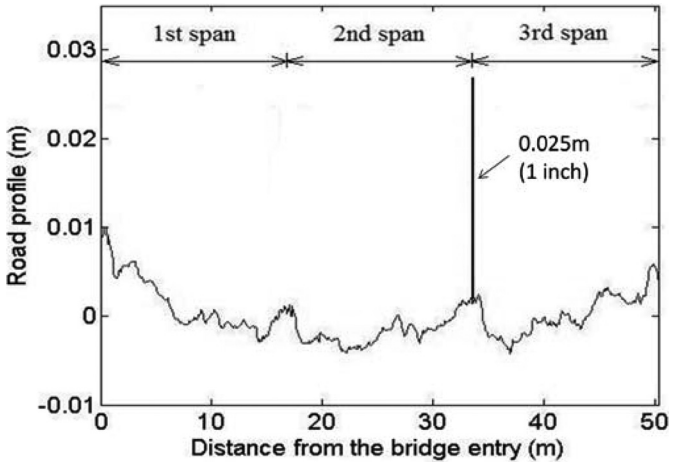

Fig. 4. Road-surface roughness along Lane 1 with Bump 1

Extraction of Bridge Frequencies

The dynamic responses of the test vehicle traveling on the bridge were calculated by analyzing the dynamic system that consisted of the test vehicle model, the updated-bridge FE model, and the measured road-surface roughness. The residual responses (accelerations) of the two trailers were calculated on the basis of the procedure shown in Fig. 2, and their FFT spectra are shown in Fig. 6 along with the acceleration spectra of Trailer 1. In addition, the conditions with and without bumps in the roughness profile were also calculated and are shown in Fig. 6. As can be seen from Fig. 6, only the trailer frequency can be identified from the acceleration spectra of Trailer 1; the first three bridge frequencies can be recognized from the spectra of the residual accelerations of the two trailers. The visibility of the trailer and bridge frequencies in the case with Bump 2 (0.038 m) is better than in the other two cases, especially for the third bridge frequency. The bump was not used to increase the roughness level but to help excite the bridge vibration, which magnifies the vehicle response as a consequence. As the bump height increases (from no bump to Bump 1 and Bump 2), the spectrum amplitudes at the bridge frequencies (B1, B2, and B3 in Fig. 6) become larger. In other words, as a result of the excitation of the bump, large responses of the test vehicle make the bridge frequencies more visible.

To further increase excitation, in addition to the tractor–trailer test vehicle, seven other traffic vehicles with different initial positions and traveling speeds were deployed in two lanes of the bridge, and the results are shown in Fig. 7. As can be seen, the amplitude at the first bridge frequency in the spectra becomes larger than that at vehicle frequency, and the visibility of the bridge frequencies become much higher than those shown in Fig. 6. The first three frequencies of the bridge, obtained from Fig. 7 (no bump), were 8.1, 11.3, and 16.8 Hz, respectively, which agree very well with the true values of 8.19, 10.79, and 16.23 Hz, respectively, indicating that the proposed method can efficiently extract the frequencies of a bridge. Compared with the condition of using only the test vehicle, the condition with ongoing traffic revealed better results, which confirms the conclusion in Kong et al. (2016). Namely, the ongoing traffic flows can provide an additional excitation to the bridge and the test vehicle and make the proposed method perform better.

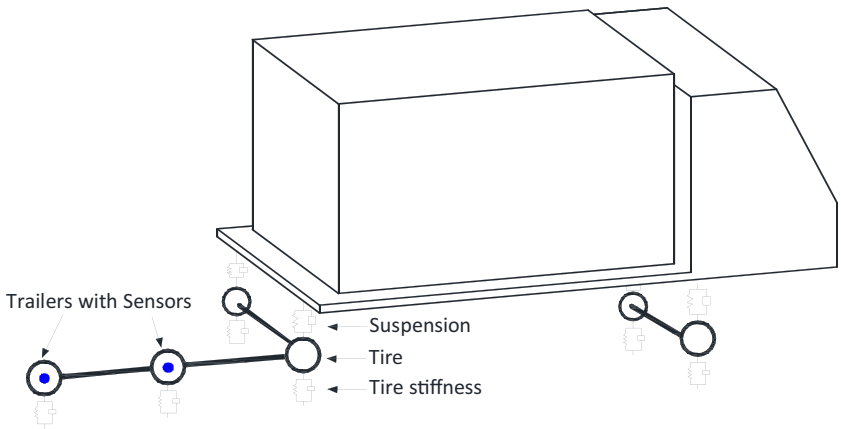

Fig. 5. Test vehicle model

Measurements in real world are always contaminated by noise from different sources. To simulate the field measurement condition, a measurement noise is typically added to the original measurements to investigate its effect. In this study, white Gaussian noise was added to the measurement to simulate sensor noise. Three levels of noises with signal-to-noise ratios (SNRs) of 40, 26, and 10 dB, which correspond to 1, 5, and 10% amplitude noise level, respectively, were considered. The noise was added to the original acceleration responses of each trailer in the case with ongoing traffic and no bump. The results are shown in Fig. 8. As can be seen, the result with 1% noise is almost the same as that of the original response shown in Fig. 7 (no bump). The result with 5% noise shows the three bridge frequencies are clearly recognizable, but with 10% noise only the first bridge frequency is obvious. The bridge frequencies identified for all the cases are listed in Table 2. The comparison shows that with approximately 5% noise, the performance of the proposed method is still acceptable.

Table 1. Main Parameters of the Dump Truck

Parameter	Value	Unit
Mass of vehicle body (M)	24,808	kg
Moments of inertia of the vehicle body (I_{zy})	31,496	kg-m^2
Moments of inertia of the vehicle body ($I_{xz} = I_{xy}$)	172,160	kg-m^2
Mass combination of tire and suspension system (m)	725.4	kg
Stiffness of the suspension systems front axle (K_{sf})	727,812	N/m
Stiffness of the suspension systems rear axle (K_{sr})	1,969,034	N/m
Damping of the suspension systems front axle (C_{sf})	2,189.6	kg/s
Damping of the suspension systems rear axle (C_{sr})	7,181.8	kg/s
Stiffness of the tires front axle (K_{tf})	1,972,900	N/m
Stiffness of the tires rear axle (K_{tr})	4,735,000	N/m
Damping of the tires front axle (C_{tf})	0	kg/s
Damping of the tires rear axle (C_{tr})	0	kg/s
Distance between front axle and the vehicle body center (L_f)	4.56	m
Distance between rear axle and the vehicle body center (L_r)	1.69	m
Distance between the two tires of the same axle (L_{ax})	2.2	m

Effects of Trailer Parameters

On the basis of the study on a simple structure, Kong et al. (2016) recommended that the frequency of the trailer should be lower than but not close to the fundamental frequency of the bridge to increase the visibility of bridge frequencies. For a specific bridge, the trailer

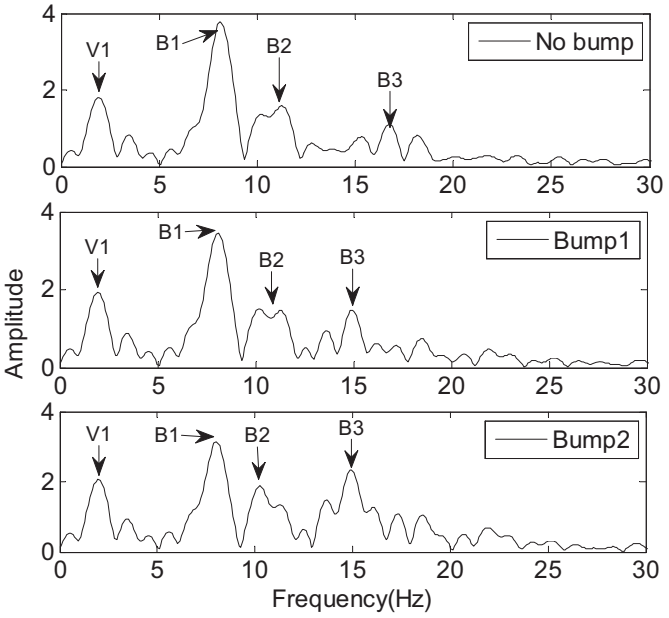

Fig. 7. FFT of residual accelerations of two trailers with ongoing traffic

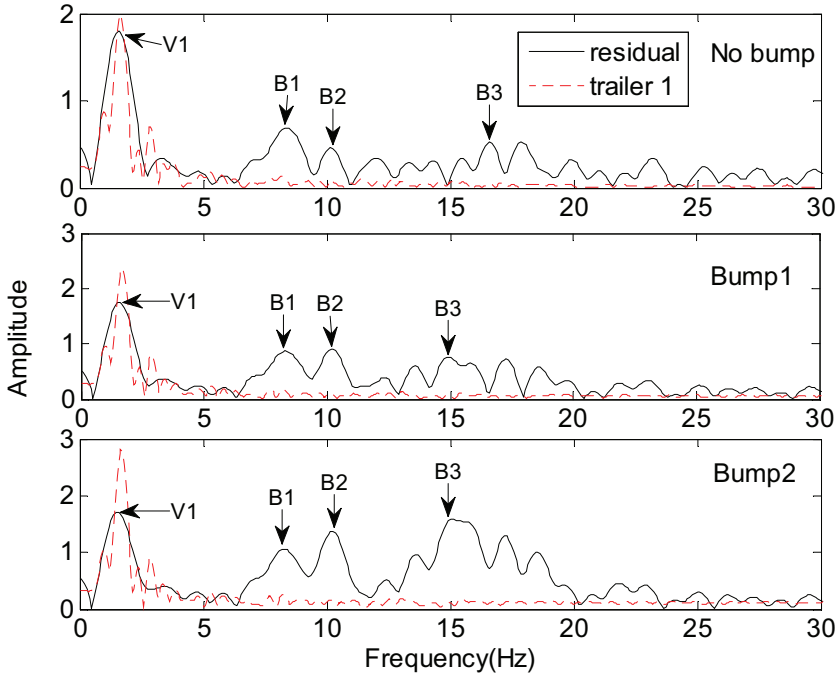

Fig. 6. Acceleration FFT of Test Vehicle Model I

parameters, such as mass and stiffness, might need to be adjusted to achieve this purpose. With respect to the studied field bridge, effects of the mass and stiffness of the trailer were investigated to design a proper trailer. Fifteen cases, as described in Tables 3 and 4, were designed. For Cases 1–8, the stiffness was fixed at 8.0×10^4 N/m, and the mass varied from 1/30 to 10 times the original mass (725.4 kg). The corresponding trailer frequencies varied from 9.155 to 0.529 Hz. In a similar fashion, for Cases 9–15, the mass was fixed at 725.4 kg, and the stiffness varied from 100 to 0.1 times the original stiffness.

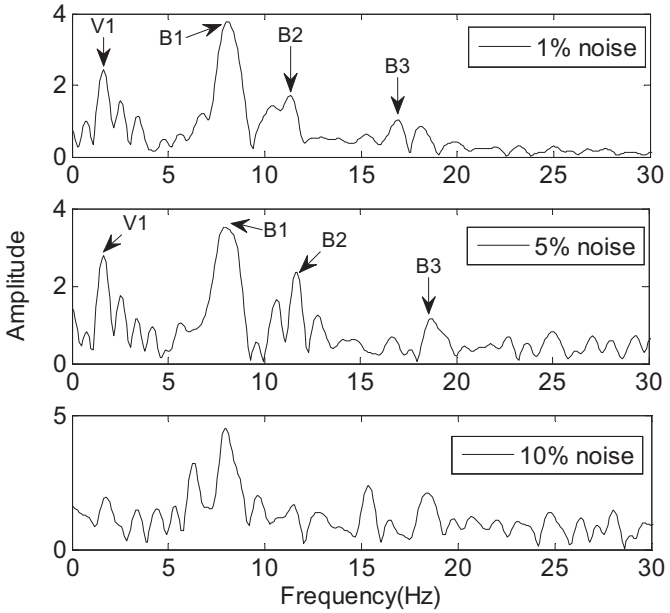

Fig. 8. FFT of residual accelerations under measurement noises

Table 2. Bridge Frequencies with Measurement Noises

Bridge frequency (noise)	Bridge frequency (Hz)		
	B1	*B2*	*B3*
None	8.10	11.30	16.80
1%	8.11	11.33	16.89
5%	8.01	11.72	18.75
10%	8.01	15.33	18.46

To evaluate the visibility of bridge frequencies in the frequency spectra, the visibility index (VI) proposed by Kong et al. (2016) was adopted; it is defined as

$$VI(\omega_i) = \frac{A(\omega_i) - \frac{1}{n}\sum_{\omega=\omega 1}^{\omega 2} A(\omega)}{\left|\frac{1}{n}\sum_{\omega=\omega 1}^{\omega 2} A(\omega)\right|} \tag{3}$$

where ω_i = ith bridge frequency; $A(\omega_i)$ = logarithmic amplitude at ω_i in the spectrum and $A(\omega)$ = logarithmic amplitude at any frequency ω in a specific frequency range; $\omega 1$ and $\omega 2$ = lower and upper limits of the frequency range used for the summation, respectively, and the values of $\omega 1 = 0.8\omega_i$ and $\omega 2 = 1.2\omega_i$ are used here; and n = number of frequencies in the range. VI, which computes the ratio of the amplitude at a specific frequency to the average amplitude at the frequency range, including that frequency, could be used to quantify the degree of difficulty in distinguishing that frequency from the spectrum.

The VIs of the first three bridge frequencies are plotted against the trailer frequencies in Figs. 9 and 10 for varied masses and stiffnesses, respectively. In Case 2, the trailer frequency was 8.357 Hz, which was very close to the bridge fundamental

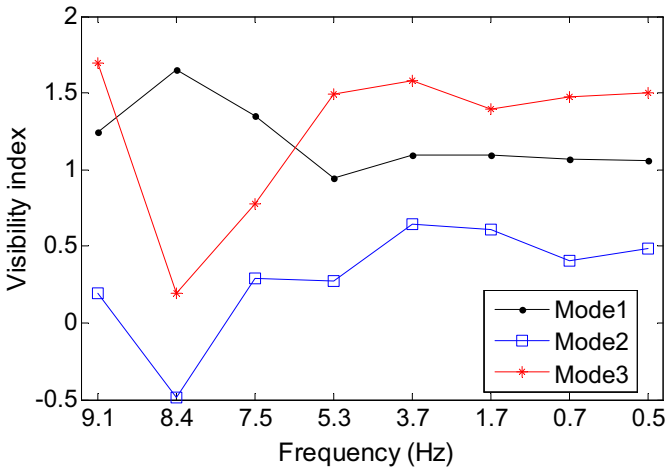

Fig. 9. Visibility index of bridge frequencies versus trailer frequency under various trailer masses

Table 3. Trailer Parameters for Cases with Different Masses

Mass change	Case							
	1	2	3	4	5	6	7	8
m_v (kg) (ratio)	24.18 (1/30)	29.02 (1/25)	36.27 (1/20)	72.54 (1/10)	145.08 (1/5)	725.40 (1)	3627 (5)	7254 (10)
k_v (N/m)	8.0×10^4							
f (Hz)	9.155	8.357	7.475	5.285	3.737	1.671	0.747	0.529

Table 4. Trailer Parameters for Cases with Different Stiffnesses

Stiffness change	Case							
	9	10	10	12	13	6	14	15
m_v (kg)	725.4							
k_v (N/m) (ratio)	8.0×10^6 (100)	4.0×10^6 (50)	2.0×10^6 (25)	8.0×10^5 (10)	4.0×10^5 (5)	8.0×10^4 (1)	4.0×10^4 (0.5)	8.0×10^3 (0.1)
f (Hz)	16.714	11.818	8.357	5.285	3.737	1.671	1.182	0.529

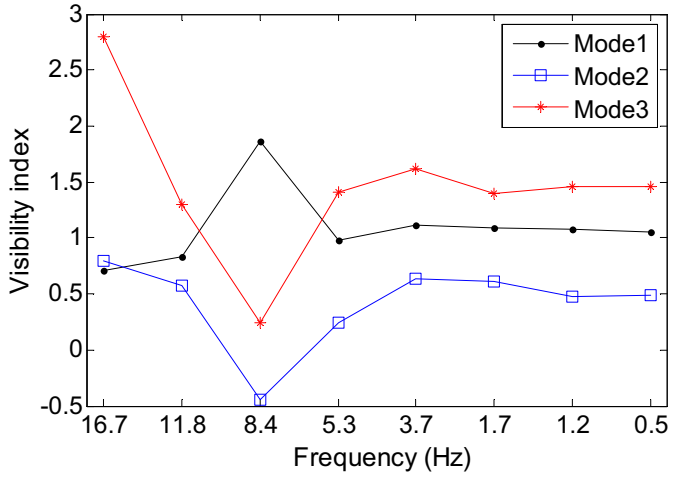

Fig. 10. Visibility index of bridge frequencies versus trailer frequency under various trailer stiffnesses

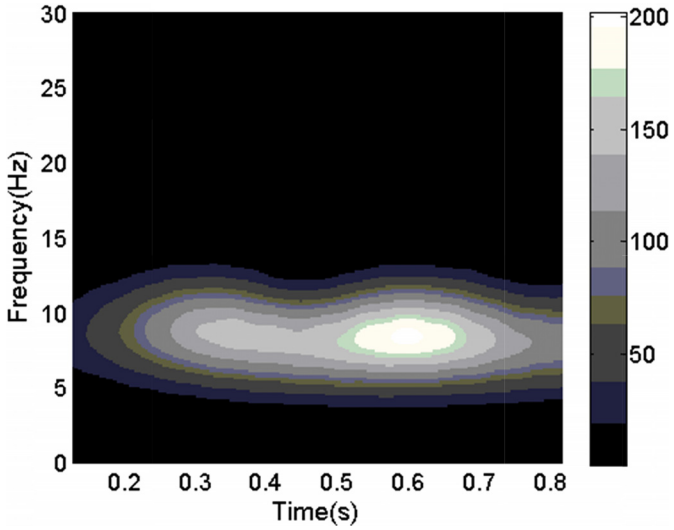

Fig. 11. STFT spectrogram of residual responses

frequency (8.19 Hz), and the VI of the first bridge frequency was much larger than that of the other two frequencies. When trailer frequencies (Cases 4–8) are smaller than the first bridge frequency, the VIs for the three bridge frequencies stay almost constant.

The same observation can be made in Fig. 10. In Case 9, with a trailer frequency of 16.714 Hz, which is close to the third bridge frequency (16.23 Hz), the VI of the third frequency was much larger than those of the other two. Meanwhile, the same trends can be observed when the trailer frequency becomes smaller than the first bridge frequency; namely, the VIs of the three bridge frequencies became almost constant. Those observations indicate that the resonance effect between the trailer and the bridge enhanced the visibility of the corresponding bridge frequency; however, it may have decreased the visibility of other bridge frequencies. Therefore, to extract more bridge frequencies, the trailer frequency was considered lower than the first bridge frequency, which confirmed the conclusion in Kong et al. (2016). Meanwhile, the trailer parameters adopted in this paper, i.e., mass of 725.4 kg and stiffness of 8.0×10^4 N/m, meet the requirement for the test bridge and are used for modal shape extraction below.

Extraction of Bridge Modal Shape Squares

As discussed, the STFT spectrogram is able to present the frequency component at different time points. Therefore, the STFT technique with a window width of 512 and overlap of 510 was applied on the residual responses of the trailers in the presence of ongoing traffic, and the results are shown in Fig. 11. The major frequency component was within the 5- to 10-Hz range, and this observation was more obvious approximately 0.2–0.75 s after the vehicle entered the bridge. The first two bridge frequencies, i.e., 8.19 and 10.79 Hz, are also in this range, which implies that the first two bridge frequencies were dominant in the residual responses of the two trailers.

The first three mode shapes from the FE analysis are shown in Fig. 12, where z, y, and x are the longitudinal, vertical, and lateral directions, respectively. The first mode was the vertical movement in the y–z plane without much bending deformation, which is caused by the unsymmetrical section of the bridge deck; the second mode is the bending movement mainly in the y–z plane; and the third mode is bending movement in the x–y plane. In contrast, on the basis of the methodology proposed in a previous study (Kong et al. 2016), the MSSs of the bridge were extracted for the first three modes (Fig. 13). All the mode shapes obtained from the FE analysis were 3D, while the MSSs extracted from the residual responses of the test vehicle were 2D. To draw a fair comparison between them, only the bridge nodes along the vehicle track were used to form the MSSs for the FE analysis. Herein, the modal displacements at the nodes along the right wheel track (4.42 m to the right shoulder) were used to form the true MSSs. All the MSSs were the vertical components. The MSSs extracted from both the STFT and FE analyses are shown in Fig. 13. Because of the configuration and support conditions of the bridge, the first three true MSSs shown in Fig. 13 look very similar and do not have the same waviness as sinusoidal modal shapes of simply supported beams. As can be seen in Fig. 13, the first and second MSSs obtained from the STFT were relatively close to the true MSSs, but the third MSSs obtained from the STFT did not quite match the true MSSs. Fig. 12 shows that the frequency components in the approximate 5- to 10-Hz range were very weak, which caused the unreasonable extraction of MSSs for the third mode (i.e., approximately 16 Hz). As shown in Fig. 12, the first two modes were mainly the vertical movement in the y–z plane, and the third mode was the bending in the x–y plane. The dominant lateral bending in the third mode could explain the reason for the differences between the extracted and true MSSs. The other possible reason could be that the true MSSs were formed from the 3D FE model, while the MSSs of the present study were extracted from the SDOF trailer with vertical responses only. A more comprehensive trailer model in which the lateral effect is considered is necessary for these kind of complex modes.

Extraction Using a More Comprehensive Test Vehicle (Model II)

In Test Vehicle Model I, the trailer was simply simulated by a SDOF vehicle. For a better simulation, a more comprehensive test vehicle model was developed by simply modifying the five-axle truck model (Cai and Chen 2004) (Fig. 14). In this model, the fourth

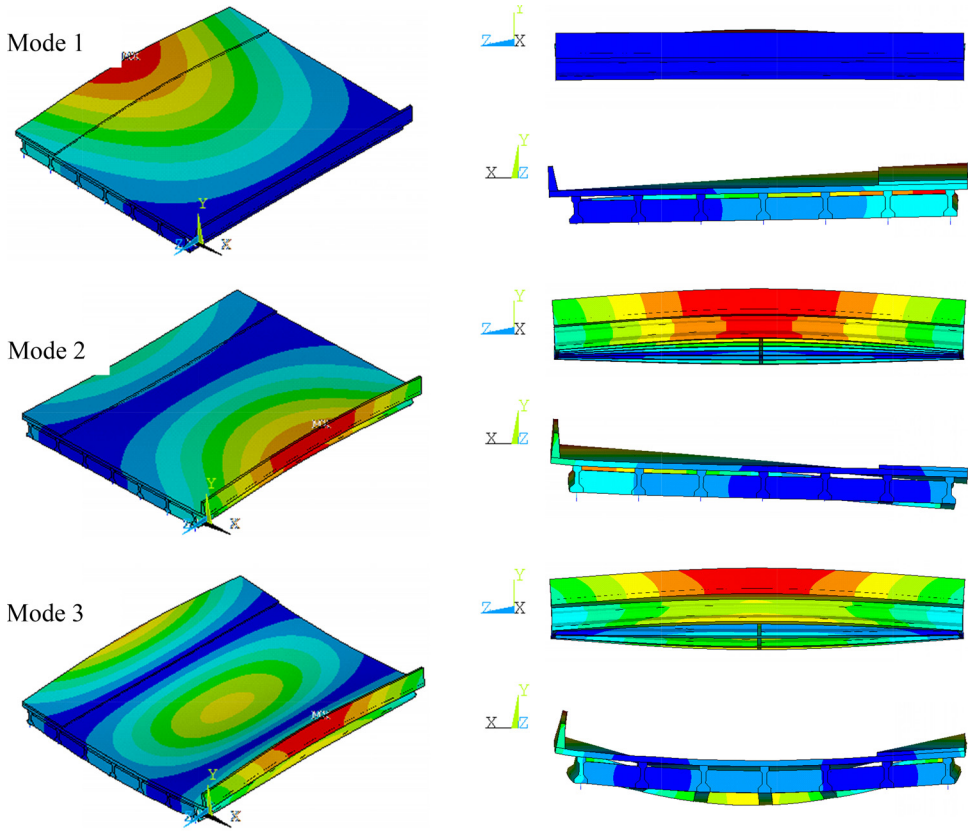

Fig. 12. Bridge modes from FE analysis

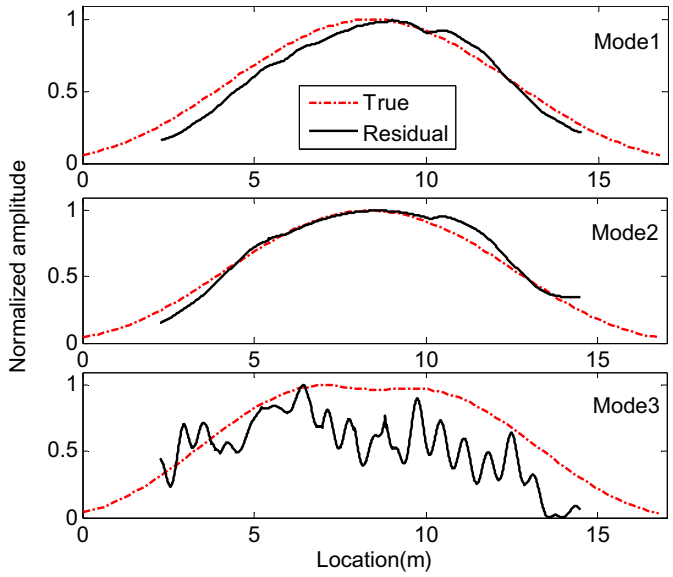

Fig. 13. Vertical MSSs of the bridge with ongoing traffic

and fifth axles were used to simulate the two trailers and the first three axles were used to simulate the tractor (i.e., the dump truck). In addition, the mass and stiffness of the rear vehicle body (Body3 in Fig. 14) were set as small values because Body3 serves only as the connection for the two axles. In this model each axle has two wheels; thus, each trailer was simulated as a 2 DOF model and has two vertical responses. The trailer parameters of Model II were the same as those in the Test Vehicle Model I, i.e., m_v was 725.4 kg, k_v was 8.0×10^4 N/m, and c_v was 2,189.6 kg/s.

Because each trailer has two wheels transversely distributed on the bridge, i.e., 6.62 m (left wheel) and 4.42 m (right wheel) to the right shoulder of the bridge deck as shown in Fig. 3, each trailer has two vertical accelerations and four accelerations can be obtained from the two trailers: A_{1L} and A_{1R} from the front trailer, A_{2L} and A_{2R} from the rear trailer (L denotes the left wheel and R denotes the right wheel). The following residual responses were considered: The residual response of accelerations from the same trailer, A_{1L}–A_{1R}, and that from two different trailers, A_{1L}–A_{2L}. The FFTs of the residual responses were normalized and shown in Fig. 15, where *B1*, *B2*, and *B3* were the true values of bridge frequencies. In the case in which no bump was used, the peak around the second bridge frequency is obvious, but the first and third frequencies cannot be as clearly identified. The results of A_{1L}–A_{1R} in this case were slightly better than those of A_{1L}–A_{2L}. However, in the cases of Bump 1 and Bump 2, the results of A_{1L}–A_{2L} were much better than those of A_{1L}–A_{1R}, and the visibilities of the first and third bridge frequencies were better than those of the second frequency. Generally speaking, the results based on the responses of the two trailers, A_{1L}–A_{2L}, were better than those in which responses of the same trailer, A_{1L}–A_{1R}, were used. This finding may be the result of the dependence of the responses of the two trailers (the four and fifth axles). As shown in Fig. 14, the pitching displacements about the lateral axis, θ_{v2} and θ_{v3}, were dependent on θ_{v1} because of the constraint equations of the two pivots. Although small stiffness and mass were used for Body3, the vertical displacements of the fourth and fifth axles were not independent. To improve this model, it is necessary to create a new vehicle that adds one additional independent DOF, i.e., the pitching displacement of Body3.

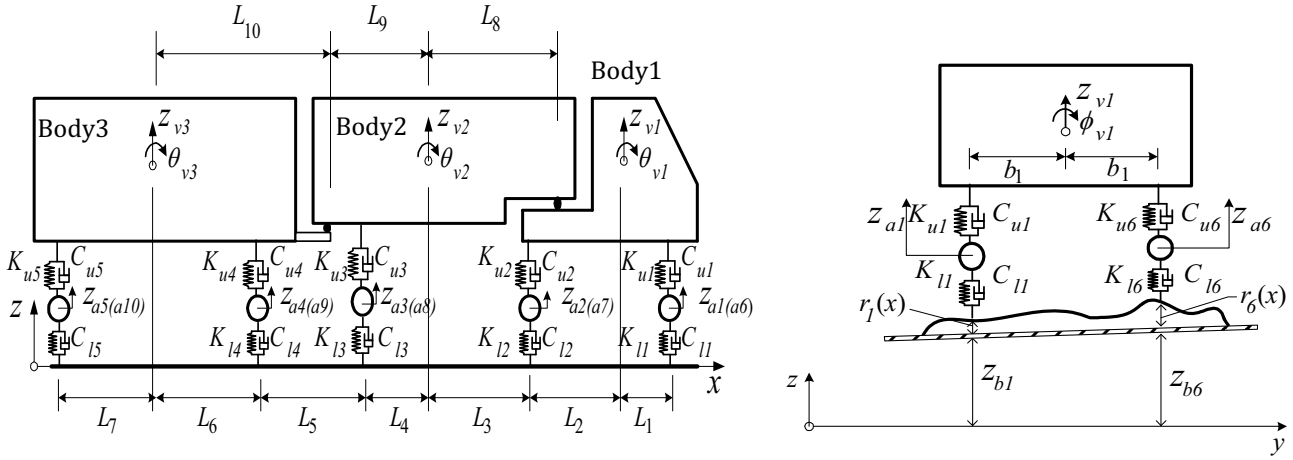

Fig. 14. Five-axle model for the test vehicle

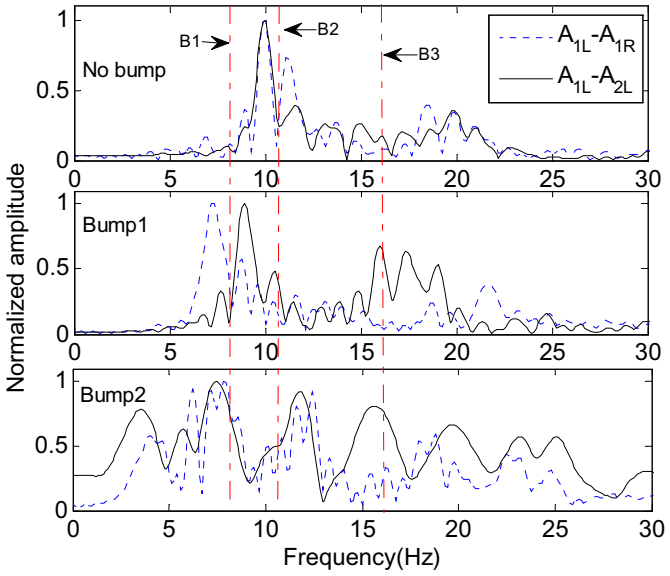

Fig. 15. FFT of residual response

Similarly, the spectrogram was obtained from residual responses, A_{1L}–A_{2L} and A_{1L}–A_{1R}, under ongoing traffic and is shown in Fig. 16. The figure clearly demonstrates that the frequency component concentrates at approximately 5–15 Hz. The left figure shows that the frequency concentration occurs continually as the vehicle travels on the bridge, but the right-hand figure shows the concentration in only the right half. In the numerical analysis, road-surface roughness for the left and right wheels was assumed to be the same, and A_{1L} and A_{1R} had no time differences. Therefore, the subtraction of A_{1L} and A_{1R} could eliminate most information, including the bridge frequency information, which could be the reason for the finding.

The MSSs of the bridge extracted from the STFT spectrogram are shown in Fig. 17 with the true MSSs obtained from the nodes along the right wheel track (4.42 m to the right shoulder). As shown in the figure, the results from A_{1L}–A_{2L} are much better than those from A_{1L}–A_{1R}. This finding implies that the residual response from the same trailer, A_{1L}–A_{1R}, was not a good option because the subtraction eliminated most of the information because no time differences were between them. In comparison, for A_{1L}–A_{2L}, the middle parts of the extracted MSSs were quite close to the true values. The discrepancies in the two end parts are possibly due to the complexity of the vehicle model and the insufficient excitation when the vehicle travels at both ends of the bridge. Compared to results of Vehicle Model I (Fig. 13), the third mode of vehicle Model II is much better. This finding implies that the more-comprehensive Vehicle Model II with multi-DOF has a better performance in extracting mode shapes dominant with lateral bending than the SDOF Vehicle Model I.

Conclusions

In the present study, an existing bridge with measured data was adopted to verify a new modal- property extraction method proposed in a previous study. The method uses a test vehicle consisting of a tractor and two following trailers to extract bridge modal properties efficiently. Two types of test vehicle models were proposed to simulate the tractor–trailer system. On the basis of the analysis, conclusions can be drawn as follows:

1. Test Vehicle Model I was established by adding two SDOF trailers to the truck model. The results show high visibility in extracted bridge frequencies. Moreover, the proposed method worked better in the presence of ongoing traffic flows that provide additional excitation to the bridge.
2. For application on the studied bridge, the effects of mass and stiffness of the trailer were investigated so a proper trailer can be designed. The resonance effect between the trailer and the bridge can benefit the visibility of the corresponding bridge frequency; however, it may decrease the visibility of other bridge frequencies. Thus, to extract more bridge frequencies, the trailer frequency is better when relatively low but not close to the first bridge frequency.
3. The MSSs extracted using Vehicle Model I matched well for the first two modes but not for the third mode. The dominant lateral bending in the third mode made it difficult to extract the MSS correctly. Because the trailer was modeled only with vertical DOF, a more comprehensive trailer model in which other DOF are considered is necessary for such complex modes.
4. A more comprehensive Test Vehicle Model II was developed by modifying the five-axle truck model, in which the fourth and fifth axles were used to simulate the two trailers. The middle parts of the extracted MSSs were quite close to the true values,

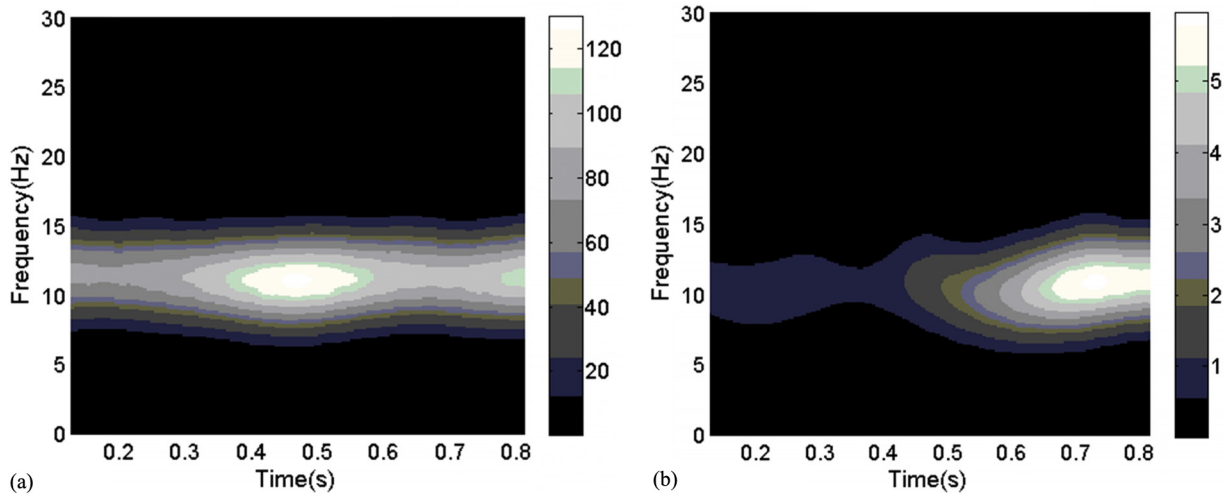

Fig. 16. STFT spectrogram of residual responses: (a) STFT from A_{1L}–A_{2L}; (b) STFT from A_{1L}–A_{1R}

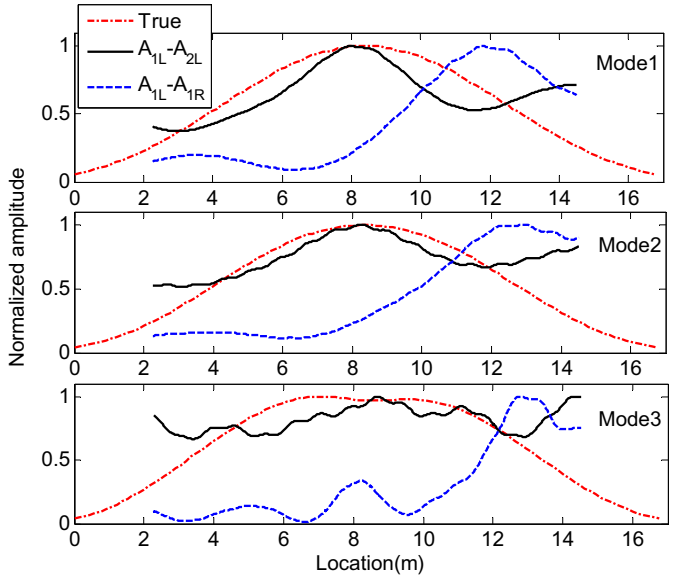

Fig. 17. MSSs of the bridge

and the discrepancies in the two end parts was possibly the result of the complexity of the vehicle model and the insufficient excitation when the vehicle travels at both ends of the bridge. However, the third MSSs extracted from A_{1L}–A_{2L} was much better than that from Vehicle Model I, which implies that Model II with multi-DOF has better performance for extracting mode shapes dominant in lateral bending than the SDOF Vehicle Model I.

In general, Vehicle Model II s more practical than Vehicle Model I, although the connection of the two trailers will affect their independence. To extract mode shapes that are not dominant in vertical movement, the lateral DOF of the trailers need to be considered and the trailer connection needs to be improved. For future work, the present study will be applied to creation of a better vehicle model to simulate the two trailers.

It may be difficult to extract high mode shapes on the basis of the proposed methodology. However, by conveniently identifying the natural frequencies and some low MSSs, this method has very practical indications for potentially quick assessments of bridge conditions.

References

ANSYS 14.5 [Computer software]. ANSYS, Canonsburg, PA.

Bu, J. Q., Law, S. S., and Zhu, X. Q. (2006). "Innovative bridge condition assessment from dynamic response of a passing vehicle." *J. Eng. Mech.*, 10.1061/(ASCE)0733-9399(2006)132:12(1372), 1372–1379.

Cai, C. S., and Chen, S. R. (2004). "Framework of vehicle–bridge–wind dynamic analysis." *J. Wind Eng. Ind. Aerodyn.*, 92(7–8), 579–607.

Cai, C. S., Shi, X. M., Araujo, M., and Chen, S. R. (2007). "Effect of approach span condition on vehicle-induced dynamic response of slab-on-girder road bridges." *Eng. Struct.*, 29(12), 3210–3226.

Carden, E. P., and Fanning, P. (2004). "Vibration based condition monitoring: A review." *Struct. Health Monit.*, 3(4), 355–377.

Curadelli, R. O., Riera, J. D., Ambrosini, D., and Amani, M. G. (2008). "Damage detection by means of structural damping identification." *Eng. Struct.*, 30(12), 3497–3504.

Das, S., Saha, P., and Patro, S. K. (2016). "Vibration-based damage detection techniques used for health monitoring of structures: A review." *J. Civ. Struct. Health Monit.*, 6(3), 477–507.

Deng, L., and Cai, C. S. (2010). "Bridge model updating using response surface method and genetic algorithm." *J. Bridge Eng.*, 10.1061/(ASCE)BE.1943-5592.0000092, 553–564.

Deng, L., and Cai, C. S. (2011). "Identification of dynamic vehicular axle loads: Demonstration by a field study." *J. Vib. Control*, 17(2), 183–195.

Doebling, S. W., Farrar, C. R., and Prime, M. B. (1998). "A summary review of vibration-based damage identification methods." *Shock Vib. Dig.*, 30(2), 91–105.

Fan, W., and Qiao, P. Z. (2011). "Vibration-based damage identification methods: A review and comparative study." *Struct. Health Monit.*, 10(1), 83–111.

González, A., Covián, E., and Madera, J. (2008). "Determination of bridge natural frequencies using a moving vehicle instrumented with accelerometers and a geographical positioning system." *Proc., 9th Int. Conf. on Computational Structures Technology*, Civil-Comp Press, Stirling, U.K.

González, A., O'Brien, E. J., and McGetrick, P. J. (2012). "Identification of damping in a bridge using a moving instrumented vehicle." *J. Sound Vib.*, 331(18), 4115–4131.

Keenahan, J., O'Brien, E. J., McGetrick, P. J., and González, A. (2014). "The use of a dynamic truck-trailer drive-by system to monitor bridge damping." *Struct. Health Monit.*, 13(2), 143–157.

Kim, C. W., Isemoto, R., Toshinami, T., Kawatani, M., McGetrick, P. J., and O'Brien, E. J. (2011). "Experimental investigation of drive-by bridge inspection." *Proc., 5th Int. Conf. on Structural Health Monitoring of Intelligent Infrastructure (SHMII-5)*, International Society for Structural Health Monitoring of Intelligent Infrastructure, Winnipeg, Manitoba, Canada.

Kong, X., Cai, C. S., and Kong, B. (2014). "Damage detection based on transmissibility of a vehicle and bridge coupled system." *J. Eng. Mech.*, 10.1061/(ASCE)EM.1943-7889.0000821, 04014102.

Kong, X., Cai, C. S., and Kong, B. (2016). "Numerically extracting bridge modal properties from dynamic responses of moving vehicles." *J. Eng. Mech.*, 10.1061/(ASCE)EM.1943-7889.0001033, 04016025.

Lin, C. W., and Yang, Y. B. (2005). "Use of a passing vehicle to scan the fundamental bridge frequencies: An experimental verification." *Eng. Struct.*, 27(13), 1865–1878.

Lu, Z. R., Huang, M., Chen, W. H., Liu, J. K., and Ni, Y. Q. (2010). "Assessment of local damages in box-girder bridges using measured dynamic responses of passing vehicle." *Prognostics and System Health Management Conf.*, IEEE Reliability Society, Piscataway, NJ.

Lu, Z. R., and Liu, J. K. (2011). "Identification of both structural damages in bridge deck and vehicle parameters using measured dynamic response." *Comput. Struct.*, 89(13–14), 1397–1405.

Lu, Z. R., Liu, J. K., Huang, M., and Xu, W. H. (2009). "Identification of damages in coupled beam systems from measured dynamic response." *J. Sound Vib.*, 326(1–2), 177–189.

Malekjafarian, A., McGetrick, P. J., and O'Brien, E. J. (2015). "A review of indirect bridge monitoring using passing vehicles." *Shock Vib.*, 286139.

McGetrick, P. J., González, A., and O'Brien, E. J. (2009). "Theoretical investigation of the use of a moving vehicle to identify bridge dynamic parameters." *Insight: Non-Dest. Test. Cond. Monit.*, 51(8), 433–438.

McGetrick, P. J., Kim, C. W., and González, A. (2013). "Dynamic axle force and road profile identification using a moving vehicle." *Int. J. Archit., Eng. Constr.*, 2(1), 1–16.

Miyamoto, A., and Yabe, A. (2011). "Bridge condition assessment based on vibration response of passenger vehicle." *J. Phys. Conf. Ser.*, 305(1), 1–10.

Sohn, H., Farrar, C., Hunter, N., and Worden, K. (2003). "A review of structural health monitoring literature: 1996-2001." *Rep., LA-13976-MS*, Los Alamos National Laboratory, Los Alamos, NM.

Yang, Y. B., and Chang, K. C. (2009a). "Extraction of bridge frequencies from the dynamic response of a passing vehicle enhanced by the EMD technique." *J. Sound Vib.*, 322(4–5), 718–739.

Yang, Y. B., and Chang, K. C. (2009b). "Extraction the bridge frequencies indirectly from a passing vehicle: Parametric study." *Eng. Struct.*, 31(10), 2448–2459.

Yang, Y. B., Chang, K. C., and Li, Y. C. (2013). "Filtering techniques for extracting bridge frequencies from a test vehicle." *Eng. Struct.*, 48(Mar), 353–362.

Yang, Y. B., Li, Y. C., and Chang, K. C. (2012). "Using two connected vehicles to measure the frequencies of bridges with rough surface: A theoretical study." *Acta Mech.*, 223(8), 1851–1861.

Yang, Y. B., Lin, C. W., and Yau, J. D. (2004). "Extracting bridge frequencies from the dynamic response of a passing vehicle." *J. Sound Vib.*, 272(3–5), 471–493.

Zhang, Y., Lie, S. T., and Xiang, Z. H. (2013). "Damage detection method based on operating deflection shape curvature extracted from dynamic response of a passing vehicle." *Mech. Syst. Signal Process.*, 35(1–2), 238–254.

Zhang, Y., Wang, L. Q., and Xiang, Z. H. (2012). "Damage detection by mode shape squares extracted from a passing vehicle." *J. Sound Vib.*, 331(2), 291–307.